Information Flow in Planar Polarity

Katherine H Fisher[1,2], Alexander G Fletcher[1,3], David Strutt[1,2,*]

1 Bateson Centre, Firth Court, University of Sheffield, S10 2TN

2 Department of Biomedical Science, Firth Court, University of Sheffield, S10 2TN

3 School of Mathematics and Statistics, Hicks Building, University of Sheffield S3 7RH

* Correspondence to d.strutt@sheffield.ac.uk

Keywords

Planar polarity, planar cell polarity, signalling, pattern formation, computational modelling, *Drosophila*

Running title: Information Flow in Planar Polarity

Abstract

Polarisation is one of the most basic levels of cell organisation. In developing tissues, sheets of cells become planar polarised – within the plane of the tissue – which is vital for coordinated cell behaviours during morphogenesis. Half a century ago, transplantation experiments revealed the ability of cells to communicate their planar polarity with their neighbours, but the underlying mechanisms remain controversial. By re-examining non-autonomous clone phenotypes in the *Drosophila* wing, coupled with computational modelling, we characterise mechanisms by which polarity information can flow bidirectionally between the polarity proteins Frizzled (Fz) and Van Gogh (Vang). Unexpectedly, our modelling suggests that local *intra*cellular feedback interactions confer directionality of information flow indirectly as a consequence of protein sorting. We conclude that directional signalling between cells depends on (i) the ability of polarity proteins to preferentially form asymmetric intercellular complexes, and (ii) the balance of feedback interactions between components of these complexes. In particular, the observed bidirectionality of signalling can be reproduced in our computational models through more than one combination of molecular wirings, suggesting avenues for future experimental investigations.

Introduction

Planar polarity and patterning of the insect cuticle

In multicellular organisms, cells in a tissue frequently adopt a common polarity such that they are oriented in the same direction in the plane of the tissue. This is termed 'planar polarity' (or planar cell polarity [PCP]) and is necessary for morphogenesis, for instance ensuring cells within a group all move or intercalate along the same tissue axis. Furthermore, planar polarity is essential for tissue function, for example when motile cilia on the surface of an epithelium all adopt the same orientation and beat in the same direction. (Reviewed in Goodrich and Strutt, 2011; Devenport, 2014; Butler and Wallingford, 2017; Davey and Moens, 2017).

Cells within a tissue could each independently establish their planar polarity by reference to an external cue such as a gradient of an extracellular signalling molecule. However, variation in signal levels across the axis of a cell might be small and difficult to discriminate, leading to individual cells mispolarising. A solution is for cells to interact: comparing and coordinating polarity with their neighbours, thus establishing uniform polarity across a field of cells even in cases where the external graded signal is weak or noisy (Ma et al., 2003; Burak and Shraiman, 2009).

Evidence for cell-cell interactions during planar polarisation was first presented by Piepho (Piepho, 1955) and Locke (Locke, 1959), who transplanted small pieces of insect cuticle and assayed the subsequent effects. The authors found that while cells normally adopt a polarity consistent with the global axes of the tissue in which they lie, if they are juxtaposed with cells attempting to adopt a different polarity then a smoothing process occurs and cells locally adopt intermediate polarities (reviewed in Strutt, 2009).

Recent studies of cell-cell interactions in planar polarity have focused on the fruit fly *Drosophila*, driven by the identification of the underlying genetic pathways. The genes regulating planar polarity in *Drosophila* have been classified into three groups: (i) the 'core' pathway; (ii) the *fat-dachsous* pathway, thought largely to act in parallel with the core pathway; (iii) genes encoding downstream 'effectors' that mediate cellular responses to the core and *fat-dachsous* pathways (reviewed in Goodrich and Strutt, 2011; Devenport, 2014).

The core planar polarity pathway

The core pathway has six known protein components, which physically interact to form intercellular complexes at apicolateral cell junctions (Fig.1A). In planar polarised tissues, these complexes are asymmetrically distributed to opposite cell ends. In the developing *Drosophila* wing, the sevenpass transmembrane protein Fz localises distally with the cytoplasmic proteins Dishevelled (Dsh) and

Diego (Dgo), whereas the fourpass transmembrane protein Vang (also known as Strabismus [Stbm]) localises proximally with the cytoplasmic protein Prickle (Pk). The sevenpass transmembrane atypical cadherin Flamingo (Fmi, also known as Starry Night [Stan]) forms intercellular homodimers and localises both proximally and distally, bridging the two halves of the complex (Strutt and Strutt, 2009) (Fig.1A).

The asymmetric distribution of these proteins specifies the distal position from which the trichome emerges in each cell (Fig.1B). Furthermore, the cellular localisation of the proteins leads to the assumption that the intercellular complexes are themselves intrinsically asymmetric, preferentially forming Fz-Fmi:Fmi-Vang and Vang-Fmi:Fmi-Fz, rather than symmetric complexes Fz-Fmi:Fmi-Fz or Vang-Fmi:Fmi-Vang (Strutt and Strutt, 2009).

The core proteins can spontaneously self-organise polarity independently of upstream 'global' cues that define the tissue axes. Most strikingly, when patches of cells lacking Fz activity are juxtaposed to cells with Fz activity during wing development, the *fz* mutant cells modify the polarity of their neighbours, whose trichomes point towards the *fz* mutant tissue (Gubb and Garcia-Bellido, 1982; Vinson and Adler, 1987). This is accompanied by relocalisation of the core proteins parallel to the clone boundary (Fig.1C) (Usui et al., 1999; Strutt, 2001; Bastock et al., 2003). Similarly, clones of cells lacking the activity of *Vang* alter the polarity of neighbouring cells, in this case causing their trichomes to point away from the mutant tissue (Fig.1D) (Taylor et al., 1998).

Such self-organisation of coordinated polarity requires cell-cell signalling, and is thus a non-cell autonomous activity. It also requires cells to amplify polarity cues to produce robust polarisation in the form of protein segregation to opposite cell ends. This amplification, through positive feedback, is regarded as a cell autonomous activity. During normal development, self-organisation is biased by upstream cues, to ensure planar polarity is correctly established along the tissue axis. In the fly wing, the nature of these upstream cues is not resolved, although multiple potential inputs have been proposed (Strutt, 2009; Aw and Devenport, 2017).

Core pathway signalling between cells: monodirectional or bidirectional?

The reorganisation of polarity around clones of cells lacking Fz and Vang, and their colocalisation on apposing junctions, suggests direct roles for these proteins in cell-cell signalling. However, loss of Fmi results in loss of all other core components from junctions (including Fz and Vang) (Strutt, 2001; Feiguin et al., 2001; Axelrod, 2001; Tree et al., 2002; Bastock et al., 2003), but does not cause significant repolarisation of neighbouring cells (Usui et al., 1999; Chae et al., 1999). Furthermore, cells with altered Fz or Vang activity, but lacking Fmi, can no longer repolarise their neighbours, and cells lacking Fmi cannot be repolarised by neighbours with altered Fz or Vang

activity (Lawrence et al., 2004; Strutt and Strutt, 2007; Chen et al., 2008). These data support the view that Fz-Fmi complexes in each cell interact with Fmi-Vang complexes in neighbouring cells, and these polarised molecular bridges are the conduits for cell-cell transmission of polarity information.

Notably, neither Dsh, Pk nor Dgo are required in cells on either side of the clone boundary for altered Fz and Vang activity to repolarise neighbouring cells (Lawrence et al., 2004; Strutt and Strutt, 2007; Chen et al., 2008). This suggests that there is no direct requirement for Dsh, Pk or Dgo activity in planar polarity cell-cell signalling.

While the roles of Fz, Vang and Fmi in cell-cell signalling are well established, there has been considerable debate regarding whether information is transmitted between cells monodirectionally from Fz to Vang, or bidirectionally between Fz and Vang (Fig.1E,F), with conflicting experimental data presented on each side. In studies on *Drosophila* abdomen hair polarity, it was reported that clones of cells with altered Fz activity (e.g. loss of Fz or Fz overexpression) could only repolarise neighbouring cells that had Vang activity (Lawrence et al., 2004), suggesting that Fz-Fmi in one cell signals monodirectionally to Fmi-Vang in the next. Further support for monodirectional signalling came from examination of the effects of clones of cells lacking both Fz and Vang activity in the *Drosophila* wing (Wu and Mlodzik, 2008). The authors concluded that *Vang*$^{-}$ *fz*$^{-}$ clones both qualitatively and quantitatively gave the same phenotype as *fz*$^{-}$ clones, again supporting monodirectional signalling from Fz-Fmi to Fmi-Vang (Fig.1E). Taken together with biochemical data revealing a physical interaction between Fz and Vang, the authors concluded that Fz is a ligand for Vang, which acts as a receptor for polarising signals.

However, other evidence argues against monodirectional signalling. Notably, cells in the wing lacking Fz activity in a *Vang*$^{-}$ background can repolarise surrounding *Vang*$^{-}$ cells (albeit only weakly), and similarly cells lacking Vang activity can weakly repolarise *fz*$^{-}$ cells (Taylor et al., 1998): thus *Vang*$^{-}$ *fz*$^{-}$ cells can influence the polarity of both *Vang*$^{-}$ and *fz*$^{-}$ cells. These results reveal an ability to signal either from Fmi to Fmi-Fz or from Fmi to Fmi-Vang in neighbouring cells, a conclusion supported by studies on bristle precursor polarisation in the fly notum (Gomes et al., 2009).

Similarly, two other studies examining *Vang*$^{-}$ *fz*$^{-}$ clones in the wing concluded that they most closely resembled *fmi*$^{-}$ clones with minimal non-autonomy (Strutt and Strutt, 2007; Chen et al., 2008). These results do not support a simple monodirectional scenario where Fz signals to Vang: instead the failure of the *Vang*$^{-}$ *fz*$^{-}$ cells to repolarise their neighbours suggests that bidirectional signalling between Fz-Fmi and Fmi-Vang coordinates polarity (Fig.1F).

Furthermore, on revisiting one of the original studies in the abdomen (Lawrence et al., 2004), Lawrence and colleagues concluded that an experimental artefact had misled them (Struhl et al., 2012). A further series of experiments instead supported bidirectional signalling between Fz-Fmi and Fmi in neighbouring cells, with Vang acting to enhance the strength of this signalling.

The weight of experimental evidence therefore favours bidirectional signalling during planar polarisation of the *Drosophila* cuticle. However, this does not imply that signalling *strength* must be the same in each direction. Indeed, studies of Fmi localisation around *fz*$^{-}$ clones in wings lacking Vang activity reveal preferential Fmi recruitment to cell boundaries between Fz expressing and non-expressing cells (Strutt and Strutt, 2008). Conversely, there is no such enhanced Fmi recruitment to boundaries of *Vang*$^{-}$ clones in wings lacking Fz activity. Furthermore, overexpressed Fmi preferentially recruits Fz to cell boundaries while apparently displacing Vang (Strutt and Strutt, 2008), and Fmi expressed in clones of cells lacking Fz and/or Vang can still recruit Fz to the boundaries of neighbouring cells (Chen et al., 2008). Together with the studies in the abdomen (Struhl et al., 2012), these findings support a model whereby Fz-Fmi:Fmi is the primary asymmetric complex that forms between the transmembrane core proteins, with Fmi:Fmi-Vang being less favoured. By extension this suggests that Fz-Fmi to Fmi signalling is stronger than Vang-Fmi to Fmi signalling.

Mechanisms of feedback amplification of polarity

Although not required for cell-cell signalling, the non-transmembrane core pathway components Dsh, Pk and Dgo are required for amplification of polarity by promoting segregation of the core protein complexes to proximal and distal cell edges. Thus loss of their activity in clones of cells results in a failure of the mutant cells to planar polarise. However, this does not cause significant repolarisation of neighbouring wild-type cells (Gubb et al., 1999; Theisen et al., 1994; Amonlirdviman et al., 2005; Strutt and Strutt, 2007).

Feedback amplification of planar polarity is most commonly assumed to occur through ‘like’ complexes of the same orientation stabilising each other, and/or ‘unlike’ complexes of opposite orientations destabilising each other (Fig.1G). Both interactions are hypothesised to result in a local build-up of complexes of the same orientation (Klein and Mlodzik, 2005; Strutt and Strutt, 2009).

A number of molecular mechanisms have been proposed to mediate such stabilising and destabilising interactions. As core proteins progressively localise into clusters of the same orientation during polarisation, it has been suggested that ‘like’ complexes may intrinsically cluster (Strutt et al., 2011; Cho et al., 2015) and that this may be driven by multiple low-affinity interactions

between core proteins leading to a phase transition into a stable state (Strutt et al., 2016). Conversely, destabilising interactions have been proposed to occur via Pk-Vang inhibiting Dsh binding to Fz (Tree et al., 2002; Amonlirdviman et al., 2005; Jenny et al., 2005), or by Pk reducing Dsh-Fz stability (Warrington et al., 2017), or by Fz-Dsh promoting Pk-mediated internalisation and turnover of Vang (Cho et al., 2015).

In parallel, numerous computational models have been proposed, implementing a variety of different feedback interactions between core protein complexes, all of which successfully recapitulate a polarised state (e.g. Amonlirdviman et al., 2005; Le Garrec et al., 2006; Burak and Shraiman, 2009; Schamberg et al., 2010). However, there is no consensus on the minimal requirements for such feedback mechanisms, or how these relate to mechanisms of cell-cell signalling.

The relationship between cell-cell signalling and feedback amplification

Although the non-transmembrane core proteins Dsh, Pk and Dgo are not required for direct cell-cell signalling, in their absence propagation of polarity across the tissue is compromised (Strutt and Strutt, 2007). Thus feedback amplification and cell-cell communication are intrinsically coupled during the establishment of planar polarity.

Bringing together the experimental observations described above, this connection between feedback amplification and cell-cell communication is illustrated by the following rationalisations of specific clone phenotypes:

fz$^-$ clones: asymmetric Fz-Fmi:Fmi-Vang complexes form strongly on clone boundaries, with Fz in the neighbouring wild-type cell localising towards the clone. The self-organising properties of the core proteins cause this mispolarisation of Fz-Fmi:Fmi-Vang to be propagated several cells away from the clone in a process that is promoted by Dsh, Pk and Dgo-dependent feedback amplification of asymmetric core protein distribution within cells (Fig.1C). *Vang*$^-$ clones behave similarly, but with Vang localised in the neighbouring cell at the clone boundary (Fig.1D).

fmi$^-$, *fmi*$^-$ *Vang*$^-$ and *fmi*$^-$ *fz*$^-$ clones: No complexes can form on the clone boundary and there is no propagation of a mispolarised state.

Vang$^-$ *fz*$^-$ clones: Fz-Fmi:Fmi complexes accumulate weakly at clone boundaries (Strutt and Strutt, 2007; Chen et al., 2008), with Fz localising in neighbouring cells on the boundary closest to the clone. This localisation can only be weakly propagated to neighbouring cells, resulting in little to no non-autonomy around clones.

Aims of the study

Our rationalisations of the observed clone phenotypes appear sufficient to explain the experimental data. However, intrinsic to these rationalisations is the assumption that bidirectional signalling does in fact occur via asymmetric intercellular core protein complexes. Moreover, contradictions in the literature regarding the phenotype of *Vang*$^-$ *fz*$^-$ clones in the wing leave open the possibility that signalling is not (or need not be) bidirectional.

Furthermore, while it appears evident that core protein asymmetric distributions driven by feedback amplification are intrinsically linked to cell-cell signalling and propagation of planar polarity, the relationship between these phenomena remains largely unexplored.

To address these issues, we have used computational modelling to explore different scenarios for core pathway function, based on different assumptions regarding protein behaviours. This, taken together with new experimental data to reassess the *Vang*$^-$ *fz*$^-$ clone phenotype, allows us to make strong predictions regarding likely molecular mechanisms of action and provides the basis for future experimental studies.

Results and Discussion

The non-autonomous phenotype of *fz*$^-$ clones is suppressed by simultaneous loss of *Vang*

We first re-examined the phenotype of clones of cells simultaneously lacking Fz and Vang activity in the *Drosophila* wing. As the *fz* and *Vang* genes lie on different chromosomes, previous studies generated double-mutant tissue using transgenes that artificially provide *fz* or *Vang* function on a different chromosome arm using exogenous promoters and which might not provide identical activity levels to the endogenous genes (Strutt and Strutt, 2007; Chen et al., 2008; Wu and Mlodzik, 2008). Thus in each study, cells lacking Fz and Vang activity are juxtaposed to neighbours with potentially differing levels of Fz and Vang activity, and this may explain the varying degrees of non-autonomous propagation of polarity reported in each case.

To circumvent the disadvantages inherent in this approach, we generated *fz*$^-$ clones in which Vang activity was either normal or was reduced only within the cells of the clone using RNAi and a MARCM GAL4/GAL80-dependent strategy (Lee and Luo, 1999 see genotypes in Materials and Methods). No transgenes were used to substitute for Fz or Vang activity, and thus the different clone genotypes should be directly comparable. RNAi expression was induced using two different *UAS-Vang-RNAi* transgenes to control for non-specific effects.

Control *fz*$^-$ clones in the pupal wing, examined shortly before or around the time of trichome formation, showed the expected strong Fz and Vang localisation at clone boundaries (Fig.2A,

arrowheads). Propagation of this aberrant polarity extended around 5-10 cells into neighbouring tissue with associated mispolarisation of trichomes pointing towards clone tissue (Fig.2B, Vinson and Adler, 1987; Strutt, 2001; Bastock et al., 2003).

In *fz*⁻ clones expressing RNAi against *Vang* transcripts, expression of either *UAS-Vang-RNAi* transgene caused loss of immunoactivity for Vang protein (Fig.2C,E). Fz and Vang recruitment to the clone boundary was suppressed (Fig.2C,E, arrowheads), and consistent with this, there were only weak effects on trichome polarity outside the clones (Fig.2D,F). In some examples with one RNAi line, trichomes partly re-orient towards the clone (Fig.2D), but never point directly towards clones (unlike with *fz*⁻ clones; compare to Fig.2B). In most cases trichomes fail to consistently re-orient towards even large clones, although trichome polarity within *fz*⁻ tissue is abnormal due to the lack of polarisation (Fig.2F).

We further considered whether the differences seen in previous reports were due to the stage at which trichome polarity was assayed, as two reports looked at pupal stages (Strutt and Strutt, 2007; Chen et al., 2008) and one analysed adult wings (Wu and Mlodzik, 2008). However, looking in adult wings in which Vang activity in *fz*⁻ clones was reduced by RNAi, we again observed a suppression of non-autonomy (compare Fig.2G,H to Fig.2J,I).

Thus, reduction in Vang activity in *fz*⁻ clones reduces Fz and Vang localisation at clone boundaries, and reduces propagation of polarity defects outside the clone, supporting previous reports that the non-autonomy of *Vang*⁻ *fz*⁻ clones is suppressed as compared to *fz*⁻ clones, and that signalling is bidirectional (Strutt and Strutt, 2007; Chen et al., 2008).

A computational modelling framework for investigating cell-cell signalling and feedback amplification in planar polarity

We have developed a computational framework to model different potential molecular mechanisms for planar polarity signalling. The framework represents a simplified system, to allow rapid scenario testing, while also attempting to capture the key features predicted from experimental data.

Within this framework, Fz and Vang represent both the transmembrane protein encoded by the corresponding gene, and the associated cytoplasmic proteins with which they interact and which are required for feedback amplification of protein asymmetry. Thus, ‘Fz’ represents Fz bound to Dsh and Dgo, and ‘Vang’ represents Vang associated with Pk. Fmi is allowed to bind homophilically in trans between neighbouring cells, and also to interact in cis with either Fz or Vang in the membranes of the same cell (Fig.S1A).

Planar polarity is simulated in a one-dimensional row of cells each with two compartments such that left and right sides represent proximal and distal membranes of each cell, respectively (Fig.S1B). In all simulations the system is initialised with one arbitrary unit (AU) of each molecular species per compartment at the start of the simulation, except that a small imbalance in initial Fz level (b; 10^{-3}) towards the right-hand (distal) side of cells provides the global orienting cue. We then numerically solve a set of ordinary differential equations describing the binding and diffusion events that occur in complex formation and localisation, evolving the system to steady state (Fig.S1B; Supplementary Text).

As discussed, there is evidence for two forms of intracellular feedback interactions: local destabilisation of 'unlike' oriented complexes, and local stabilisation of 'like' oriented complexes (Fig.1G). Destabilising feedback interactions were implemented such that Vang-containing complexes (Vang-Fmi:Fmi and Vang-Fmi:Fmi-Fz) in each cell compartment destabilised Fz-containing complexes (Fz-Fmi:Fmi and Fz-Fmi:Fmi-Vang) in the same compartment, and vice versa. The strength of each destabilising feedback, originating from either Fz or Vang, was controlled by the V_{max} parameters, $V_{max,F}$ and $V_{max,V}$, respectively. These parameters represent the maximum fold-change conferred to the off-rate of each reaction (see Box 1 and Supplementary Text). Stabilising feedback interactions were implemented in a similar manner, such that Vang- or Fz-containing complexes stabilised themselves through increase of their binding reaction on-rates.

After exploring both destabilising and stabilising feedback interactions in simulations, we concluded that in general these mechanisms polarised the system equivalently. However, while stabilising feedbacks recapitulated key clone phenotypes, there were subtle differences in some cases (see Supplementary Text for further discussion and Fig.S2A,B). For systems relying only on stabilising feedbacks, 'unlike' complex stability was unchanged, thus the system was slower to polarise and more sensitive to the rate of protein diffusion. Hereafter, we consider models with destabilising feedbacks only.

Once a steady state was reached, wild-type polarity was defined as higher Fz bound into complexes at distal cell ends and higher Vang bound at proximal cell ends (Fig.S1C). For particular models, we first identified conditions giving a polarised steady state across the row of cells. We then tested the effect on local polarity of introducing clones of cells lacking the activity of one or more factors, specifically *fz*$^-$, *Vang*$^-$, *Vang*$^-$ *fz*$^-$ and *fmi*$^-$. We quantified non-autonomy around the clone as the number of cells with reversed polarisation in terms of Fz localisation (although, in general, results were the same if we instead quantified Vang localisation). A reversal of polarity in cells on the right-hand side of a clone, such that Fz pointed towards the clone, was referred to as distal non-autonomy (i.e. a *fz*-like phenotype), while polarity reversals on the left side were called proximal non-autonomy (*Vang*-like).

We have systematically tested sensitivity of these phenotypes to variations in each parameter (see Supplementary Text). We found that only two parameters had a significant effect on the direction of any observed non-autonomy around clones: (i) the relative dissociation constants (K_D) for binding between Fmi, Fz and Vang in junctions, and (ii) the strength of the feedback interactions between Fz and Vang, parameterised by $V_{max,F}$ and $V_{max,V}$ respectively.

We identified models (Table 1) and associated parameter sets (Table S1) that reproduced *in vivo* observations based on the following criteria: *fz*⁻ clones gave distal non-autonomy for several cell diameters, beyond which this was replaced with normal polarity as specified by the global cue; *Vang*⁻ clones resulted in proximal non-autonomy for several cell diameters; *Vang*⁻ *fz*⁻ clones caused no or weak distal non-autonomy (over a smaller range than equivalent *fz*⁻ clones); and *fmi*⁻ clones caused no or weak proximal non-autonomy. We deliberately have not tested the effect of overexpressing proteins, as it is difficult to predict in particular contexts whether an overexpressed protein is acting to increase or decrease normal protein function.

Asymmetric complexes without direct signalling (Model 1: bidirectional feedbacks)

Previous data have been interpreted such that symmetric complexes (Fz-Fmi:Fmi-Fz and Vang-Fmi:Fmi-Vang) are assumed to form a negligible pool of all complexes. This assumption has been made in previous computational models (Amonlirdviman et al., 2005; Le Garrec et al., 2006). Thus, in our first model (Table 1: Model 1), we did not allow formation of symmetric complexes. This was achieved by setting the relevant binding rate constants (k_6, k_7) to zero (i.e. 'switching off' reactions 6 and 7 in Fig.3A). In this case the allowed complexes between neighbouring cells were Fmi:Fmi, Fz-Fmi:Fmi, Fmi:Fmi-Vang and Fz-Fmi:Fmi-Vang, the latter three having either orientation (Fig.3A).

Within this model there was no direct communication between cells. We term such models 'no signalling', meaning that a cell is unable to directly 'sense' the levels of Fz or Vang in its neighbours when complexes form. Complex formation was implemented in the model by allowing Fmi to bind at cell-cell interfaces to form dimers, and allowing both Fz and Vang to bind to and stabilise these dimers; however, no additional stability was conferred to a complex if Fz bound once Vang was already present on the other side of the dimer (i.e. the same K_D value for reactions 2 and 5 in Fig.3A), or vice versa (i.e. the same K_D value for reactions 3 and 4 in Fig.3A). Thus, Fz and Vang could not promote each other's incorporation into intercellular complexes. We therefore did not expect mutant clones to show non-autonomy in this model.

Cells could polarise through feedback amplification of the initial global cue (i.e. the small imbalance in Fz to the distal side of each cell). Since molecular evidence for local destabilising feedback

interactions both from Fz to Vang and from Vang to Fz have been reported in the literature (Tree et al., 2002; Jenny et al., 2005; Cho et al., 2015; Warrington et al., 2017), both were implemented in this model, by setting the values of $V_{max,F}$ and $V_{max,V}$ to greater than 1 (see Box 1; Fig.3B).

We first set out to establish parameter values (Table S1) that generated wild-type polarity in Model 1, where Fz complexes accumulated on distal cell edges and Vang complexes accumulated on proximal cell edges (Fig.3C; Fig.S1C). We then examined the behaviour of loss-of-function clones in this model. We hypothesised that under the 'no signalling' assumption, this model would not generate non-autonomy around clones of cells with altered Fz or Vang activity, since no direct signalling occurred between cells.

Surprisingly, despite the lack of direct signalling across complexes, we found that for most parameter sets recapitulating wild-type polarity, *fz*$^-$ clones showed distal non-autonomy (Fig.3D,E) and *Vang*$^-$ clones showed proximal non-autonomy (Fig.3F,G). Furthermore, both *Vang*$^-$ *fz*$^-$ clones (Fig.3H,I) and *fmi*$^-$ clones (Fig.3J,K) were autonomous, thus reproducing the anticipated outcomes for bidirectional signalling. For *fmi*$^-$ clones, non-autonomy did not propagate beyond the first cell neighbouring the clone: this cell could only localise its Fz and Vang to its edge furthest from the clone. Thus, in the first cell proximal to the clone Fz polarity was reversed and in the first cell distal to the clone Vang polarity was reversed (Fig.3J). Since we quantified non-autonomy based on Fz repolarisation, we scored this as one cell proximal non-autonomy (Fig.3K); were we scoring Vang repolarisation, this would be scored as having one cell distal non-autonomy.

The range of non-autonomy was a function of both the strength of the initial Fz bias (*b*) and the strength of feedback (V_{max}). Higher values of either parameter suppressed non-autonomy, since the amplification of the initial bias in each cell dominated over the mislocalisation of protein complexes propagating from the clone edge (Fig.3E,G,I,K; see Supplementary Text).

This unexpected 'indirect bidirectional signalling' (and consequent non-autonomy around *fz*$^-$ and *Vang*$^-$ clones) arose as a result of only allowing intrinsically asymmetric complexes to form. At each cell-cell junction, binding of Vang to a Fmi:Fmi dimer in one cell was blocked if Vang was bound to the same dimer in the neighbouring cell (since symmetric Vang-Fmi:Fmi-Vang complexes were not allowed to form), and similarly for Fz.

To illustrate the consequences of only allowing asymmetric complexes to form, we first considered the example of a *fz*$^-$ clone. On the boundary between a *fz*$^-$ clone and a neighbouring wild-type cell, only Vang could bind to Fmi:Fmi on the inner clone boundary, and Fz binding on the outer clone boundary in the wild-type cell was favoured over Vang binding (as Vang-Fmi-Fmi-Vang complexes could not form, Fig.S3A). This generated an imbalance whereby more Fz bound to the outer clone

boundary than Vang, and more Vang bound to the inner clone boundary (Fig.S3A). This imbalance could be seen as the system evolved to steady state in the absence of any feedbacks (Fig.S3B), and was amplified when introducing feedback interactions between Fz and Vang, resulting in propagation of Fz mislocalisation pointing towards the clone (Fig.3D).

Around *Vang*$^-$ clones, the same occurred in reverse: with Vang binding to the outer clone boundary being favoured over Fz, and feedback amplifying this difference (Fig.S3C; Fig.3F). Around *Vang*$^-$ *fz*$^-$ clones, Fz and Vang could both bind to Fmi:Fmi dimers at the outer clone boundary with equal affinity and thus attained equal levels at clone boundaries in the absence of feedback (Fig.S3D). Similarly for *fmi*$^-$ clones, since no binding could occur at the clone boundary, Fz and Vang were equally localised to the next boundary along in the absence of feedback (Fig.S3E). Since the feedback interactions were bidirectional and operated with equal strength, Fz and Vang destabilised each other equally, thus there was no net polarity cue and no repolarisation around the clone.

Hence, with no direct signalling (Fz and Vang do not directly promote each other's binding within the same complex [as in Fig.3A]), and bidirectional feedback (between Fz and Vang, and Vang and Fz [as in Fig.3B]), this model qualitatively reproduced the experimental observations. Model 1 provides an example of a possible molecular wiring in core pathway planar polarity signalling.

<u>Asymmetric complexes without direct signalling (Model 2: single feedback; Model 3: unbalanced feedbacks)</u>

To confirm that 'indirect bidirectional signalling' is dependent on bidirectional feedbacks of equal strength between Fz and Vang, we asked whether adapting our model to include only a single intracellular feedback operating would show monodirectionality and hence produce non-autonomy around *Vang*$^-$ *fz*$^-$ clones. We kept the same assumptions as for Model 1, except we implemented only one of the destabilising feedbacks, originating either from Fz or Vang (Table 1: Model 2). It should be noted that when using a single feedback, the parameter values were altered to ensure that cells were able to polarise in wild-type simulations (see Supplementary Text; Table S1).

In these single feedback models, *fz*$^-$ or *Vang*$^-$ clones gave the expected non-autonomy (Fig.4A,B). Again, this is simplest to understand when examining steady states in the absence of feedback. As we have already shown, cells immediately neighbouring the clones were polarised in the absence of feedback (cells 5 and 11; Fig.S3B,C), and either of the single feedback interactions were capable of propagating this (Fig.4A,B).

Interestingly, *Vang*$^-$ *fz*$^-$ double clones resembled either a *Vang*$^-$ clone, when only feedback from Vang was acting (Fig.4A), or a *fz*$^-$ clone when only feedback from Fz was operating (Fig.4B), as

would be predicted for monodirectional signalling. This can be explained as follows: in cells neighbouring these double clones, Fz and Vang bound equally to Fmi:Fmi dimers, but only one of them could destabilise the other through the single destabilising feedback operating. Thus the molecule that is not subject to any feedback destabilisation 'wins' on that boundary, resulting in the observed non-autonomy (Fig.S4A). We refer to this as 'indirect monodirectional signalling'.

Finally, we examined *fmi*$^-$ clones in Model 2. Simulations showed non-autonomy, but in the opposite direction to *Vang*$^-$ *fz*$^-$ clones (Fig.4A,B). In cells neighbouring *fmi*$^-$ clones, the immediate boundary was unable to localise any complexes due to the inability to form Fmi:Fmi dimers, as seen when simulating complex formation in the absence of feedback (Fig.S3E). Since all of the proteins in such cells had to localise to the boundary furthest from the clone, the protein mediating the feedback 'won' on this boundary (Fig.S4B). For instance, Fz accumulated on the boundary furthest from the clone when it was able to destabilise Vang, and Vang accumulated away from the clone when it could destabilise Fz (Fig.S4B).

We next adapted the model to examine two feedbacks operating with different strengths (Table 1: Model 3; Table S1). We found that while single *fz*$^-$ or *Vang*$^-$ clones behaved as expected, this again introduced some non-autonomy around *Vang*$^-$ *fz*$^-$ clones (Fig.4C,D). If stronger feedback was operating from Vang, then the non-autonomy was proximal (Fig.4C), but distal non-autonomy was evident if feedback was stronger from Fz (Fig.4D): the molecule with the strongest destabilising role 'won' on a boundary generating the non-autonomy (Fig.S4A), with the degree of non-autonomy depending on the strength of each feedback used (Table S2). Around *fmi*$^-$ clones, we saw similar results to that of single feedback models, such that non-autonomy was opposite to *Vang*$^-$ *fz*$^-$ clones (Fig.4C,D; Fig.S4B).

We conclude that in simulations where intrinsically asymmetric complexes were present, the presence of two opposing feedback interactions resulted in indirect bidirectional signalling (with the balance of the feedbacks determining the balance of the directionality; Table 1: Model 1), whereas a single feedback resulted in indirect monodirectional signalling (Table 1: Model 2). Thus, the single feedback scenarios can be ruled out as possible *in vivo* mechanisms in the *Drosophila* wing, as they fail to reproduce the observed weak or absent non-autonomous phenotypes of *Vang*$^-$ *fz*$^-$ and *fmi*$^-$ clones. However, a weak distal non-autonomy around *Vang*$^-$ *fz*$^-$ double clones is consistent with experimental data (Strutt and Strutt, 2007; Chen et al., 2008; Strutt and Strutt, 2008; Struhl et al., 2012), and may suggest that *in vivo* there is stronger feedback operating from Fz-Dsh compared to Vang-Pk (Fig.4D).

Asymmetric complexes without direct signalling (Model 1: bidirectional feedback. Clones without feedback)

Loss-of-function clones of the cytoplasmic proteins are cell autonomous (Theisen et al., 1994; Gubb et al., 1999; Amonlirdviman et al., 2005; Strutt and Strutt, 2007). The interpretation of this behaviour has been that cytoplasmic proteins are involved in intracellular feedback interactions and thus do not play a role in communication between cells. However, our simulations suggest that feedback can alter this communication indirectly.

While we did not model the cytoplasmic proteins explicitly, we could simulate their absence by inhibiting feedback within clones (Table 1: Model 1). Removal of one of the feedbacks within a clone (by setting $V_{max,F}$ or $V_{max,V}$ to 1 within those cells), stopping Vang from destabilising Fz or vice versa, resulted in either proximal or distal non-autonomy around the clone (Fig.4E,F). However, if we removed both feedbacks from within a clone the system became balanced and thus, autonomous (Fig.4G): as seen for *dsh* and *pk* clones *in vivo* (Gubb et al., 1999; Theisen et al., 1994; Amonlirdviman et al., 2005; Strutt and Strutt, 2007).

We conclude that in scenarios where bidirectional signalling resulted from the presence of two opposing feedbacks (i.e. Vang destabilises Fz *and* Fz destabilises Vang), loss of either Dsh or Pk needed to block *both* feedbacks in order for Model 1 to recapitulate *in vivo* phenotypes. We speculate that this would be the case if Vang destabilisation of Fz was mediated by Pk acting on Dsh, and Fz destabilisation of Vang was mediated by Dsh acting on Pk, consistent with previous reports (Tree et al., 2002; Jenny et al., 2005; Cho et al., 2015).

Symmetric and asymmetric complexes with direct signalling (Models 4-6: bidirectional feedback)

The most notable feature of Models 1 and 2 is the ability of intrinsically asymmetric complex formation, coupled with feedback interactions, to mediate indirect signalling between neighbouring cells, enabling them to sense the presence of Fz and/or Vang. Having tested the effects of disrupting feedbacks in this system, we next examined the requirement for intrinsically asymmetric complexes.

Previous experimental evidence has been interpreted to suggest that Fz, Vang and Fmi exclusively form asymmetric complexes, or at least that asymmetric complexes are highly favoured (Chen et al., 2008; Strutt and Strutt, 2008; Wu and Mlodzik, 2008; Struhl et al., 2012). Similarly, previous computational models have only included the existence of asymmetric complexes, although Le Garrec (2006) comment that asymmetric complexes need only be more likely to form than symmetric ones for the system to behave as presented. It is generally assumed that conformational changes transmitted via Fmi:Fmi dimers ensure that once Fz or Vang is bound,

then only the other partner can bind to the opposite half of the dimer: but this seems unlikely to be an 'all or nothing' process. Instead it is plausible that both symmetric and asymmetric complexes form but conformational changes lead to asymmetric complexes being favoured. In this context, it is interesting to note that in contact inhibition during vertebrate embryo development, symmetric complexes involving Fz-Dsh are thought to be active at cell-cell contacts (Carmona-Fontaine et al., 2008).

We therefore revised our modelling assumption that intercellular complexes were intrinsically asymmetric, instead allowing symmetric Fz-Fmi:Fmi-Fz and Vang-Fmi:Fmi-Vang complexes to form in addition to asymmetric Fz-Fmi:Fmi-Vang complexes (Table 1: Models 4-6). We maintained balanced bidirectional feedbacks to ensure that any changes to non-autonomy were purely a result of allowing symmetric complexes to form. Three different scenarios were tested:

(i) 'No direct signalling' between Fz and Vang (Table 1: Model 4). As implemented above, this was simulated by allowing Fmi:Fmi to bind at cell-cell interfaces to form dimers, and allowing both Fz and Vang to bind to and stabilise these dimers, such that all complexes involving Fz or Vang had equal K_D (Fig.5A).

(ii) 'Direct monodirectional signalling' from Fz to Vang (Table 1: Model 5). This was implemented by Vang bound to a Fmi:Fmi-Fz complex having a very low dissociation constant, but Fz bound to a Fmi:Fmi-Vang complex having the same intermediate dissociation constant as Fz bound to just Fmi:Fmi. Thus localisation of Vang at junctions was promoted by Fz in the next cell, but Fz was unaffected by Vang in the next cell (Fig.5A).

(iii) 'Direct bidirectional signalling' between Fz and Vang (Table 1: Model 6). In this case, both Vang bound to a Fmi:Fmi-Fz complex and Fz bound to a Fmi:Fmi-Vang complex had low dissociation constants, but Vang bound to Fmi:Fmi and Fz bound to Fmi:Fmi had intermediate dissociation constants. Thus Fz and Vang both promoted each other's binding in the next cell (Fig.5A).

In the 'no direct signalling' case (Table 1: Model 4), consistent with a lack of communication across cell interfaces, and unlike our model with only asymmetric complexes (Table 1: Model 1), we saw no significant non-autonomy around *fz*$^-$, *Vang*$^-$, *Vang*$^-$ *fz*$^-$ or *fmi*$^-$ clones (Fig.5B-E). To illustrate this, we considered the possible complexes that could form on the boundary of a *fz*$^-$ clone. We have seen that for models with only asymmetric complexes more Fz accumulated on the outer clone boundary (Model 1, Fig.S3A), however, allowing symmetric complexes to form led to equal amounts of Fz and Vang and thus no accumulation of either protein (Model 4, Fig.S5A). This balance between Fz and Vang could be seen when evolving the system to steady state in the

absence of any feedbacks for each type of clone (Fig.S5B-E). In each case, Fz and Vang levels were equal to one another on each cell boundary outside of the clone (Fig.S5B-E; cells 11 and 12). In this model, since Fz or Vang binding in one cell was not influenced by availability of Fz or Vang in a neighbouring cell, the initial bias in Fz levels was the driving force for polarisation, amplified by feedback.

'Direct monodirectional signalling' (Table 1: Model 5) resulted in distal and proximal non-autonomy around *fz*$^-$ and *Vang*$^-$ clones, respectively (Fig.5F,G). This can be rationalised by considering that Vang binds preferentially to complexes containing Fz in the next cell. Thus, on the *fz*$^-$ clone boundary, Vang inside the clone bound preferentially into complexes containing Fz in the bordering wild-type cells. Furthermore, Vang in the bordering wild-type cells preferentially localised away from the clone (Fig.S6A, orange arrows). Consistent with this, when simulating a *fz*$^-$ clone in the absence of feedback, we observed Vang localising on boundaries furthest away from the clone (Fig.S6B). The converse was true for *Vang*$^-$ clones with Vang in neighbouring cells preferentially localising towards the clone (Fig.S6C).

As expected for monodirectional signalling (see Introduction), distal non-autonomy was observed around *Vang*$^-$ *fz*$^-$ clones (Fig.5H), consistent with Vang being sensitive to Fz bound in the next cell. In cells immediately neighbouring *Vang*$^-$ *fz*$^-$ clones, Vang preferentially bound to Fz-containing complexes and thus accumulated on the boundary furthest from the clone (Fig.S6D, orange arrows). This accumulation was observed when evolving the model to steady state in the absence of feedback (Fig.S6E). Here, both Fz and Vang were seen to localise away from the clone in cell 11, but Vang was at higher levels than Fz. This in turn recruited Fz and Vang to the boundary in the neighbouring cell (left side of cell 12), with Fz reaching higher levels than Vang. In the presence of feedback, this small asymmetry in complex formation drove the resultant distal non-autonomy.

Within this model of 'direct monodirectional signalling' (Model 5) we found that *fmi*$^-$ clones showed distal non-autonomy (Fig.5I). We again considered steady state behaviour in the absence of feedback for an explanation. In cells immediately next to the clone (Fig.S6F; 5 and 11), both Fz and Vang localised away from the clone. However, Vang preferentially bound to Fz-containing complexes and thus, as for *Vang*$^-$ *fz*$^-$ clones, accumulated on the boundary furthest from the clone to higher levels than Fz (Fig.S6G, orange arrows).

In the 'direct bidirectional signalling' model (Table 1: Model 6), distal and proximal non-autonomy were again observed around *fz*$^-$ and *Vang*$^-$ clones, respectively (Fig.5J,K). We rationalised these phenotypes by looking at the complexes that could form in the cells immediately neighbouring the clone in the absence of any feedback. For example, in cells next to a *fz*$^-$ clone, Vang and Fz both

preferentially localised towards cells with their binding partner, Fz and Vang, respectively. Since there was no Fz within the clone, Vang accumulated on boundaries furthest from the clone (Fig.S7A, orange arrows; Fig.S7B). The converse was true for *Vang*⁻ clones with Fz accumulating away from the clone in neighbouring cells (Fig.S7C). However, around *Vang*⁻ *fz*⁻ clones, neither Fz nor Vang binding to cell boundaries on the clone edge was favoured, resulting in no non-autonomy around clones (Fig.5L). In this case, both Fz and Vang accumulated away from the clone in search of their binding partner, but neither outcompeted the other (Fig.S7D,E). Model 6 also recapitulated the expected phenotype of *fmi*⁻ clones, showing no propagating non-autonomy by the same rationale (Fig.5M, Fig.S7F) and was therefore a good fit for the experimental observations.

In summary, we have demonstrated that by introducing formation of symmetric complexes into the system, we are able to disrupt the 'indirect signalling' observed in Models 1-3. By altering binding affinities of particular intercellular complexes, we are able to introduce 'direct signalling' between cells and alter the nature of this signalling. For example, we have shown that bidirectional signalling could be mediated indirectly via asymmetric complexes and bidirectional feedbacks (Model 1), or, in the presence of symmetric complexes, directly via changes in binding affinities of intercellular complex components, such that Fz and Vang are both sensitive to levels of the other in neighbouring cells (Model 6). Furthermore, we could simulate monodirectional signalling either indirectly with asymmetric complexes and a single feedback operating (Model 2), or in the presence of symmetric complexes, by direct manipulation of binding affinities for a particular complex – i.e. that Vang is more stable when Fz is present in the neighbouring cell (Model 5).

<u>Preferential binding of Fmi to Fz (Model 7: bidirectional feedbacks; Model 8 single feedback)</u>

We have identified models that show purely bidirectional signalling and result in no non-autonomy around *Vang*⁻ *fz*⁻ clones (Table1: Models 1 and 6). However, as previously noted, there is evidence to support the view that *in vivo* Fz-Fmi:Fmi complexes are favoured over Vang-Fmi:Fmi complexes. We therefore studied whether implementing such a scenario in Model 1 had a significant impact on clone phenotypes. To achieve this, we slightly reduced the dissociation constant (K_D) for all Fz binding reactions, making Fz inherently better at binding to Fmi than Vang, regardless of whether Vang was already part of the complex (Table 1: Model 7; Fig.6A). Hereafter we refer to this as a Fz binding bias. The binding bias was considered to get stronger as the Fz binding dissociation constant was decreased (see labels in Fig.6B). We did not allow symmetric complexes to form in this case and we initally implemented *both* destabilising feedbacks (from Fz to Vang and from Vang to Fz).

We found that *fz*⁻ (Fig.6B) and *Vang*⁻ clones (Fig.6C) again showed distal and proximal non-autonomy, respectively, as expected. However, *Vang*⁻ *fz*⁻ double clones showed weak distal non-

autonomy in the presence of a weak bias (Fig.6D). The binding bias did not alter the result for *fmi*⁻ clones, which still showed one cell proximal non-autonomy (Fig.6E). These results suggest that a weak Fz binding bias is able to offer directionality to the system, reinforcing one of the feedbacks. Furthermore, it gave a possible mechanism by which weak distal non-autonomy might be generated around *Vang*⁻ *fz*⁻ clones.

We next tested whether a Fz binding bias could act to *replace* one of the feedbacks in this model. We therefore removed the feedback where Fz acts to destabilise Vang (by setting $V_{max,F}$ to 1; Table 1: Model 8). This scenario is similar to conditions in a previous model by Amonlirdviman et al (2005; see also Fischer et al., 2013), which included one destabilising feedback (Pk and/or Stbm on Dsh) as well as a binding bias (Dsh-Fz binding had a lower off rate than Fz alone).

We have previously examined the role of this single feedback interaction (Vang destabilising Fz) in the absence of any binding bias (Model 2, Fig.4A). When introducing a Fz binding bias (Model 8), we initially maintained the parameter value for the feedback interaction (i.e. $V_{max,V}$ = 40). We found that introducing a binding bias did not alter the amount or direction of non-autonomy observed around *fz*⁻ or *Vang*⁻ clones (Fig.6F,G, compare to Fig.4A). However, *Vang*⁻ *fz*⁻ clones showed non-autonomy varying from proximal to distal as the Fz binding bias increased (Fig.6H) and for a small parameter range, no non-autonomy was observed (e.g. K_D = 0.018 in Fig.6H). It should be noted that a stronger Fz binding bias was required to see any effect as compared to Model 7.

We suggest that this varying non-autonomy occurred due to the precise balance between the feedback interaction from Vang and the Fz binding bias. At the boundary to a *Vang*⁻ *fz*⁻ clone, only two complexes could form – Fz-Fmi:Fmi and Vang-Fmi:Fmi (Fig.S8A). The Fz binding bias would favour the formation of the Fz complex: however, this complex was also destabilised by the feedback from Vang. If the binding bias was weak, the feedback dominated and Vang accumulated at the clone boundary resulting in proximal non-autonomy (Fig.S8A). If the Fz binding bias balanced with the strength of the feedback, then neither Vang nor Fz outcompeted the other and no non-autonomy occurred (Fig.S8B). If, however, the binding bias was strong, Fz was not sufficiently destabilised by feedback from Vang, and Fz accumulated on this boundary, resulting in distal non-autonomy (Fig.S8C).

To test our deductions further, we examined clone phenotypes within the model in the presence of a weaker feedback from Vang (achieved by reducing $V_{max,V}$). As previously observed, reducing the feedback strength increased the amount of non-autonomy around *fz*⁻ or *Vang*⁻ clones, but did not alter the direction (Fig.S8D,E). We found that *Vang*⁻ *fz*⁻ clones still showed a switch from proximal to distal non-autonomy as the binding bias was increased, but, as predicted, a weaker bias (i.e. a

K_D of 0.05 compared to the previous 0.018) was necessary to balance the weaker feedback (Fig.S8F).

These findings suggest that for a small parameter range a Fz binding bias could act to replace one of the feedback interactions to generate apparent bidirectionality in the system. However, these conditions resulted in non-autonomy around *fmi*$^-$ clones. Using the same parameter values for Fz binding bias yielding varying non-autonomy around *Vang*$^-$ *fz*$^-$ clones (Fig.6H; note that $V_{max,V}$ = 40), we observed distal non-autonomy around *fmi*$^-$ clones (Fig.6I). We found that this was also the case when using a weaker feedback interaction ($V_{max,V}$ = 10; Fig.S8G). Since distal non-autonomy is never observed around *fmi*$^-$ clones *in vivo*, we conclude that this model (Model 8) does not reflect a possible molecular wiring underlying planar polarity signalling.

In summary, the apparent preference for Fz-Fmi:Fmi binding over Fmi:Fmi-Vang binding seen *in vivo* is predicted to result in weak non-autonomous phenotypes around *Vang*$^-$ *fz*$^-$ clones *in vivo* and may underlie some of the non-autonomy reported by Wu & Mlodzik (2008). However, while such a binding bias can add directionality, it cannot completely replace one of the feedbacks required to obtain bidirectional signalling.

Conclusions

We set out to understand the possible molecular wirings that might underlie the cell-cell coordination of planar polarity. We specifically address possible scenarios that would explain the observed behaviour of the core planar polarity pathway in the *Drosophila* wing, but our findings also reveal other scenarios that could coordinate polarity in other contexts.

By carrying out new experiments examining the double *Vang*$^-$ *fz*$^-$ clone phenotype in the wing, we confirm that non-autonomy is suppressed when compared to either *fz*$^-$ or *Vang*$^-$ single mutant clones, supporting bidirectional signalling between Fz and Vang. Simulations indicate that this bidirectional signalling can be mediated either *indirectly* via intrinsically asymmetric intercellular protein complexes and bidirectional feedbacks, or *directly* via different affinities for protein binding in intercellular complexes (Table 1).

Monodirectional signalling – mediated either *indirectly* via intrinsically asymmetric intercellular protein complexes and monodirectional feedback, or *directly* via different affinities for protein binding in intercellular complexes – is able to polarise a tissue and reproduce the phenotypes of single mutant *fz*$^-$ and *Vang*$^-$ clones. However, in no cases we examined could monodirectional signalling reproduce the observed weak, or complete lack of, non-autonomy around double mutant *Vang*$^-$ *fz*$^-$ clones or single mutant *fmi*$^-$ clones.

Experimental data suggest that *in vivo* Fmi binds more strongly to Fz than to Vang. We find that this can bias the direction of signalling and give non-autonomy around *Vang*$^{-}$ *fz*$^{-}$ clones, but does not eliminate the requirement for bidirectional feedbacks to reproduce *in vivo* behaviours.

Further support for the presence of bidirectional feedbacks *in vivo* comes from our attempts to simulate clones lacking activity of the cytoplasmic core proteins Pk and Dsh. These are believed to be involved in mediating destabilising feedback interactions, but clones of cells lacking their activity *in vivo* do not result in non-autonomy. We are only able to reproduce this finding in our models if both proteins are involved in bidirectional feedback interactions.

Overall, our work suggests that while many binding and feedback regimes can generate polarity and reproduce *fz*$^{-}$ and *Vang*$^{-}$ clone phenotypes, *Vang*$^{-}$ *fz*$^{-}$ clones and *fmi*$^{-}$ clones are key simulations required to constrain model parameters to mirror the *in vivo* reality. We define a minimum set of conditions that reproduce the observed *in vivo* phenotypes. Nevertheless, as multiple feedbacks and biases can offer directionality to the overall signalling system it is plausible that *in vivo* more than one mechanism contributes to the observed robust polarisation.

We suggest that future experimental studies should focus on two questions. First, what are the molecular parameters of intercellular complex formation and do these support formation of intrinsically asymmetric complexes and/or direct signalling between Fz and Vang? Second, what is the molecular nature of the feedback interactions and (minimally) can two opposing feedbacks be identified between Fz- and Vang-containing complexes?

Materials and Methods

Drosophila genetics

Mitotic clones were generated using the *fz*^{P21} allele, which is considered to be a null (Jones et al., 1996), using the MARCM system (Lee and Luo, 1999) and *Ubx-FLP* (Emery et al., 2005). Here, *tub-GAL4* and *UAS-GFP* were expressed in every cell, but *tub-GAL80* suppressed expression of *UAS-GFP* in heterozygous or twin-spot tissue only, thus GFP was only observed in *fz*$^{-}$ clone cells. To generate *Vang*$^{-}$ *fz*$^{-}$ double clones, *UAS-Vang-RNAi* transgenes were introduced distal to *fz* on chromosome 3L, such that they also would only be expressed within clones. Strength of Vang knockdown was visualised by staining for Vang. We used a line from the TRiP collection (HMS01343) and a *pWIZ* line (Bastock and Strutt, 2007). Full genotypes were:

Fig.2A,B,G,H:

Ubx-FLP tubGAL4 UAS-nGFP/+ ; fz^{P21} *FRT80 / tubGAL80 FRT80*

Fig.2C,D:

Ubx-FLP tubGAL4 UAS-nGFP/+ ; UAS-Vang-RNAi$^{(pWIZ)}$ *FRT80 / tubGAL80 FRT80*

Fig.2E,F,I,J:

Ubx-FLP tubGAL4 UAS-nGFP/+ ; UAS-Vang-RNAi$^{(TRiP)}$ *fz*^{P21} *FRT80 / tubGAL80 FRT80*

Dissection and Immunohistochemistry

White prepupae were collected and aged as appropriate at 25˚C. Pupal wings were dissected at either 28 h APF to visualise polarity protein localisation, or at 32.25 h APF for trichomes. Pupal wings were then fixed and stained as previously described (Warrington et al., 2017). Briefly, pupae were fixed for 30-45 minutes at room temperature, prior to dissection of the pupal wing. Wings were transferred into PBS containing 0.2% Triton X-100 (PTX) and 10% normal goat serum to block prior to antibody incubation. Wings were incubated with antibodies overnight at 4°C, and mounted in 10% glycerol, 1xPBS, containing 2.5% DABCO (pH7.5). Primary antibodies for immunostaining were affinity purified rabbit anti-GFP (ab6556, Abcam, UK), affinity-purified rabbit anti-Fz (Bastock and Strutt, 2007), rat anti-Vang (Strutt and Strutt, 2008) and mouse monoclonal anti-Fmi (Flamingo #74, DSHB, (Usui et al., 1999)). Trichomes were stained using Phalloidin conjugated to Alexa-568 (Molecular Probes). Adult wings were dissected from newly eclosed flies and transferred to a 10 µl drop of PTX in a depression slide for imaging.

Imaging

Fixed pupal wings were imaged on a Nikon A1R GaAsP confocal microscope using a 60x NA1.4 apochromatic lens, with a pixel size of 138 nm, and the pinhole was set to 1.2 AU. 9 Z-slices separated by 150 nm were imaged, and then the 3 brightest slices around junctions were selected and averaged for each channel in ImageJ. Adult wings were imaged on a fluorescence compound microscope to capture trichomes in brightfield and GFP to mark clonal cells. Since brightfield and GFP signals were in different planes, single slices were selected and realigned in Adobe Photoshop.

Computational modelling

A detailed description of the model equations, assumptions, conditions, and parameters can be found in the Supplementary Text. Briefly, the computational model comprises a set of coupled ordinary differential equations, which encode intercellular binding reactions between core proteins/complexes and intracellular diffusion in a one-dimensional line of cells aligned along a proximodistal axis. This set of equations is solved numerically using an explicit Runge-Kutta method. A MATLAB implementation will be deposited in GitHub.

Acknowledgements

The authors would like to thank Helen Strutt and Simon Fellgett for comments on the manuscript. We also acknowledge the Bloomington *Drosophila* Stock Center for providing fly strains. The work was funded by a Wellcome Senior Fellowship award (grant number WT100986/Z/13/Z) to DS.

Competing interests

None.

References

Amonlirdviman, K., Khare, N.A., Tree, D.R., Chen, W.S., Axelrod, J.D., and Tomlin, C.J. (2005). Mathematical modeling of planar cell polarity to understand domineering nonautonomy. Science *307*, 423-426.

Aw, W.Y., and Devenport, D. (2017). Planar cell polarity: global inputs establishing cellular asymmetry. Curr Opin Cell Biol *44*, 110-116.

Axelrod, J.D. (2001). Unipolar membrane association of Dishevelled mediates Frizzled planar cell polarity signaling. Genes Dev *15*, 1182-1187.

Bastock, R., and Strutt, D. (2007). The planar polarity pathway promotes coordinated cell migration during Drosophila oogenesis. Development *134*, 3055-3064.

Bastock, R., Strutt, H., and Strutt, D. (2003). Strabismus is asymmetrically localised and binds to Prickle and Dishevelled during *Drosophila* planar polarity patterning. Development *130*, 3007-3014.

Burak, Y., and Shraiman, B.I. (2009). Order and stochastic dynamics in *Drosophila* planar cell polarity. PLoS Comput Biol *5*, e1000628.

Butler, M.T., and Wallingford, J.B. (2017). Planar cell polarity in development and disease. Nat Rev Mol Cell Biol *18*, 375-388.

Carmona-Fontaine, C., Matthews, H.K., Kuriyama, S., Moreno, M., Dunn, G.A., Parsons, M., Stern, C.D., and Mayor, R. (2008). Contact inhibition of locomotion in vivo controls neural crest directional migration. Nature *456*, 957-961.

Chae, J., Kim, M.J., Goo, J.H., Collier, S., Gubb, D., Charlton, J., Adler, P.N., and Park, W.J. (1999). The *Drosophila* tissue polarity gene *starry night* encodes a member of the protocadherin family. Development *126*, 5421-5429.

Chen, W.S., Antic, D., Matis, M., Logan, C.Y., Povelones, M., Anderson, G.A., Nusse, R., and Axelrod, J.D. (2008). Asymmetric homotypic interactions of the atypical cadherin Flamingo mediate intercellular polarity signaling. Cell *133*, 1093-1105.

Cho, B., Pierre-Louis, G., Sagner, A., Eaton, S., and Axelrod, J.D. (2015). Clustering and negative feedback by endocytosis in planar cell polarity signaling is modulated by ubiquitinylation of Prickle. PLoS Genet *11*, e1005259.

Davey, C.F., and Moens, C.B. (2017). Planar cell polarity in moving cells: think globally, act locally. Development *144*, 187-200.

Devenport, D. (2014). The cell biology of planar cell polarity. J Cell Biol *207*, 171-179.

Emery, G., Hutterer, A., Berdnik, D., Mayer, B., Wirtz-Peitz, F., Gaitan, M.G., and Knoblich, J.A. (2005). Asymmetric Rab 11 endosomes regulate delta recycling and specify cell fate in the *Drosophila* nervous system. Cell *122*, 763-773.

Feiguin, F., Hannus, M., Mlodzik, M., and Eaton, S. (2001). The ankyrin repeat protein Diego mediates Frizzled-dependent planar polarization. Dev Cell *1*, 93-101.
Fischer, S., Houston, P., Monk, N.A., and Owen, M.R. (2013). Is a persistent global bias necessary for the establishment of planar cell polarity? PLoS One *8*, e60064.
Gomes, J.E., Corado, M., and Schweisguth, F. (2009). Van Gogh and Frizzled act redundantly in the *Drosophila* sensory organ precursor cell to orient its asymmetric division. PLoS One *4*, e4485.
Goodrich, L.V., and Strutt, D. (2011). Principles of planar polarity in animal development. Development *138*, 1877-1892.
Gubb, D., and Garcia-Bellido, A. (1982). A genetic analysis of the determination of cuticular polarity during development in *Drosophila melanogaster*. J Embryol Exp Morphol *68*, 37-57.
Gubb, D., Green, C., Huen, D., Coulson, D., Johnson, G., Tree, D., Collier, S., and Roote, J. (1999). The balance between isoforms of the Prickle LIM domain protein is critical for planar polarity in *Drosophila* imaginal discs. Genes Dev *13*, 2315-2327.
Jenny, A., Reynolds-Kenneally, J., Das, G., Burnett, M., and Mlodzik, M. (2005). Diego and Prickle regulate Frizzled planar cell polarity signalling by competing for Dishevelled binding. Nat Cell Biol *7*, 691-697.
Jones, K.H., Liu, J., and Adler, P.N. (1996). Molecular analysis of EMS-induced *frizzled* mutations in *Drosophila melanogaster*. Genetics *142*, 205-215.
Klein, T.J., and Mlodzik, M. (2005). Planar Cell Polarization: An Emerging Model Points in the Right Direction. Annu Rev Cell Dev Biol *21*, 155-176.
Klunder, B., Freisinger, T., Wedlich-Soldner, R., and Frey, E. (2013). GDI-mediated cell polarization in yeast provides precise spatial and temporal control of Cdc42 signaling. PLoS Comput Biol *9*, e1003396.
Lawrence, P.A., Casal, J., and Struhl, G. (2004). Cell interactions and planar polarity in the abdominal epidermis of *Drosophila*. Development *131*, 4651-4664.
Le Garrec, J.F., Lopez, P., and Kerszberg, M. (2006). Establishment and maintenance of planar epithelial cell polarity by asymmetric cadherin bridges: a computer model. Dev Dyn *235*, 235-246.
Lee, T., and Luo, L. (1999). Mosaic analysis with a repressible cell marker for studies of gene function in neuronal morphogenesis. Neuron *22*, 451-461.
Locke, M. (1959). The Cuticular Pattern in an Insect, Rhodnius-Prolixus Stal. J Exp Biol *36*, 459-476.
Ma, D., Yang, C.H., McNeill, H., Simon, M.A., and Axelrod, J.D. (2003). Fidelity in planar cell polarity signalling. Nature *421*, 543-547.
Piepho, H. (1955). Uber Die Ausrichtung Der Schuppenbalge Und Schuppen Am Schmetterlingsrumpf. Naturwissenschaften *42*, 22-22.
Schamberg, S., Houston, P., Monk, N.A., and Owen, M.R. (2010). Modelling and analysis of planar cell polarity. Bull Math Biol *72*, 645-680.

Struhl, G., Casal, J., and Lawrence, P.A. (2012). Dissecting the molecular bridges that mediate the function of Frizzled in planar cell polarity. Development *139*, 3665-3674.
Strutt, D. (2009). Gradients and the specification of planar polarity in the insect cuticle. Cold Spring Harb Perspect Biol *1*, a000489.
Strutt, D., and Strutt, H. (2007). Differential activities of the core planar polarity proteins during *Drosophila* wing patterning. Dev Biol *302*, 181-194.
Strutt, D.I. (2001). Asymmetric localization of Frizzled and the establishment of cell polarity in the *Drosophila* wing. Mol Cell *7*, 367-375.
Strutt, H., Gamage, J., and Strutt, D. (2016). Robust Asymmetric Localization of Planar Polarity Proteins Is Associated with Organization into Signalosome-like Domains of Variable Stoichiometry. Cell Rep *17*, 2660-2671.
Strutt, H., and Strutt, D. (2008). Differential stability of Flamingo protein complexes underlies the establishment of planar polarity. Curr Biol *18*, 1555-1564.
Strutt, H., and Strutt, D. (2009). Asymmetric localisation of planar polarity proteins: Mechanisms and consequences. Semin Cell Dev Biol *20*, 957-963.
Strutt, H., Warrington, S.J., and Strutt, D. (2011). Dynamics of core planar polarity protein turnover and stable assembly into discrete membrane subdomains. Dev Cell *20*, 511-525.
Taylor, J., Abramova, N., Charlton, J., and Adler, P.N. (1998). *Van Gogh*: a new *Drosophila* tissue polarity gene. Genetics *150*, 199-210.
Theisen, H., Purcell, J., Bennett, M., Kansagara, D., Syed, A., and Marsh, J.L. (1994). *dishevelled* is required during *wingless* signaling to establish both cell polarity and cell identity. Development *120*, 347-360.
Tree, D.R., Shulman, J.M., Rousset, R., Scott, M.P., Gubb, D., and Axelrod, J.D. (2002). Prickle mediates feedback amplification to generate asymmetric planar cell polarity signaling. Cell *109*, 371-381.
Usui, T., Shima, Y., Shimada, Y., Hirano, S., Burgess, R.W., Schwarz, T.L., Takeichi, M., and Uemura, T. (1999). Flamingo, a seven-pass transmembrane cadherin, regulates planar cell polarity under the control of Frizzled. Cell *98*, 585-595.
Vinson, C.R., and Adler, P.N. (1987). Directional non-cell autonomy and the transmission of polarity information by the *frizzled* gene of *Drosophila*. Nature *329*, 549-551.
Warrington, S.J., Strutt, H., Fisher, K.H., and Strutt, D. (2017). A Dual Function for Prickle in Regulating Frizzled Stability during Feedback-Dependent Amplification of Planar Polarity. Curr Biol *27*, 2784 - 2797.e2783.
Wu, J., and Mlodzik, M. (2008). The Frizzled extracellular domain is a ligand for Van Gogh/Stbm during nonautonomous planar cell polarity signaling. Dev Cell *15*, 462-469.

Box 1 - *Model parameters*

Binding rate constants: Mass action binding rates are proportional to the product of reactants in any reaction. Forward reaction rates are parameterised by rate constants k_1 to k_7, and reverse reactions by v_1 to v_7. The relative reaction rates are thus determined by the dissociation constant K_D calculated by v_j/k_j.

Diffusion: In a 1D model where each cell has just two compartments, diffusion is modelled by a linear flux between these compartments. The rate of this flux is parameterised by $D = \mu/L^2$, where μ is the diffusion coefficient, estimated at 0.03 $\mu m^2 s^{-1}$ (Fischer et al., 2013; Klunder et al., 2013) and L is the distance between compartments, estimated at 5 µm.

Feedback: Destabilising feedback is modelled by a Hill function of the form $h(x) = 1 + (V_{max} - 1)[x]^w/(K^w + [x]^w)$, where $[x]$ is the amount of protein x mediating the feedback.

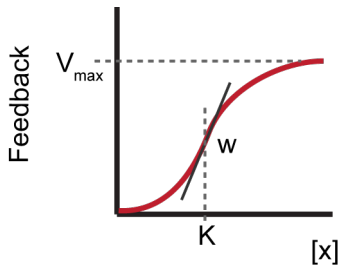

The parameter V_{max} determines the strength of the feedback as the maximum fold-change that can be conferred to the off-rate of each reaction. Since feedback can be mediated by either Fz or Vang, strength of feedback is determined by $V_{max,F}$ or $V_{max,V}$, respectively. K determines the amount of protein x required to switch from weak to strong feedback and w determines the rate of this switch. We set K to 0.5, which is half of the initial concentration of Fz and Vang in each compartment. A higher value of w reflects cooperativity such that a small increase in $[x]$ can cause large differences in its ability to destabilise complexes. Since we do not have evidence of enzymatic ability in these reactions which may cause such cooperativity, we aimed to maintain w as low, keeping it at 2 where possible.

All parameters are listed in Table S1 and further discussion of model sensitivity to these parameters can be found in the Supplementary Text.

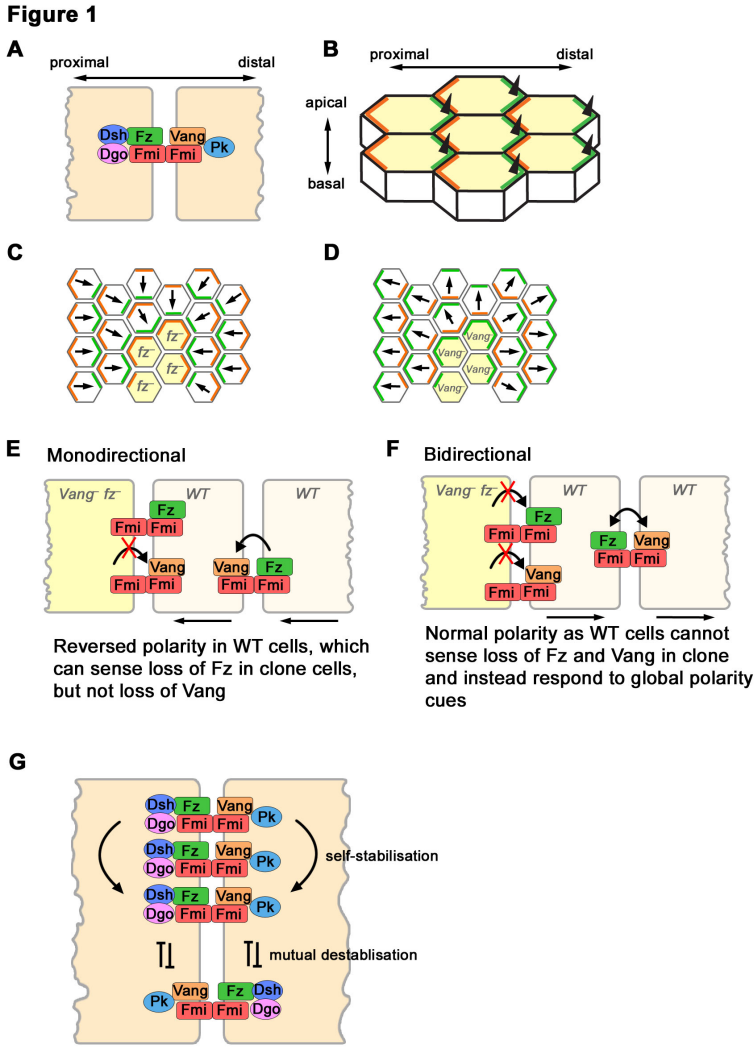

Figure 1. Directional signalling in planar polarity.

(A) Diagram of the core planar polarity proteins localising to form an intercellular complex at a junction between two cells.

(B) Diagram showing asymmetric localisation of Fz (green) and Vang (orange) in the developing *Drosophila* wing. Black triangles represent trichomes emerging at distal cell ends.

(C,D) Diagrams of non-autonomous phenotypes of *fz*⁻ (C) and *Vang*⁻ (D) clones (yellow cells) in pupal wings. Arrows represent trichome orientation. At the edge of a *fz*⁻ clone, Vang within the clone cells localises to the boundary with wild-type neighbours, indicating it preferentially forms asymmetric complexes with Fz at cell-cell contacts. The same is the case for Fz localising at the boundary of *Vang*⁻ clones.

(E,F) Monodirectional (E) and bidirectional (F) signalling predictions. In monodirectional signalling (E), Vang acts as a ligand for Fz and can 'sense' its levels in neighbouring wild-type (WT) cells. *Vang*⁻ *fz*⁻ clones behave identically to *fz*⁻ clones, since no information on Vang levels is transmitted

between cells. In bidirectional signalling (F), no information can be passed from *Vang*$^{-}$ *fz*$^{-}$ cells since both are required for sending and receiving the signal. Thus neighbouring wild-type cells are blind to the clone and polarise normally.

(G) Diagram of possible feedback interactions. Stabilising interactions occur locally between complexes of ‘like’ orientations, whereas destabilising interactions occur between complexes of ‘unlike’ orientations.

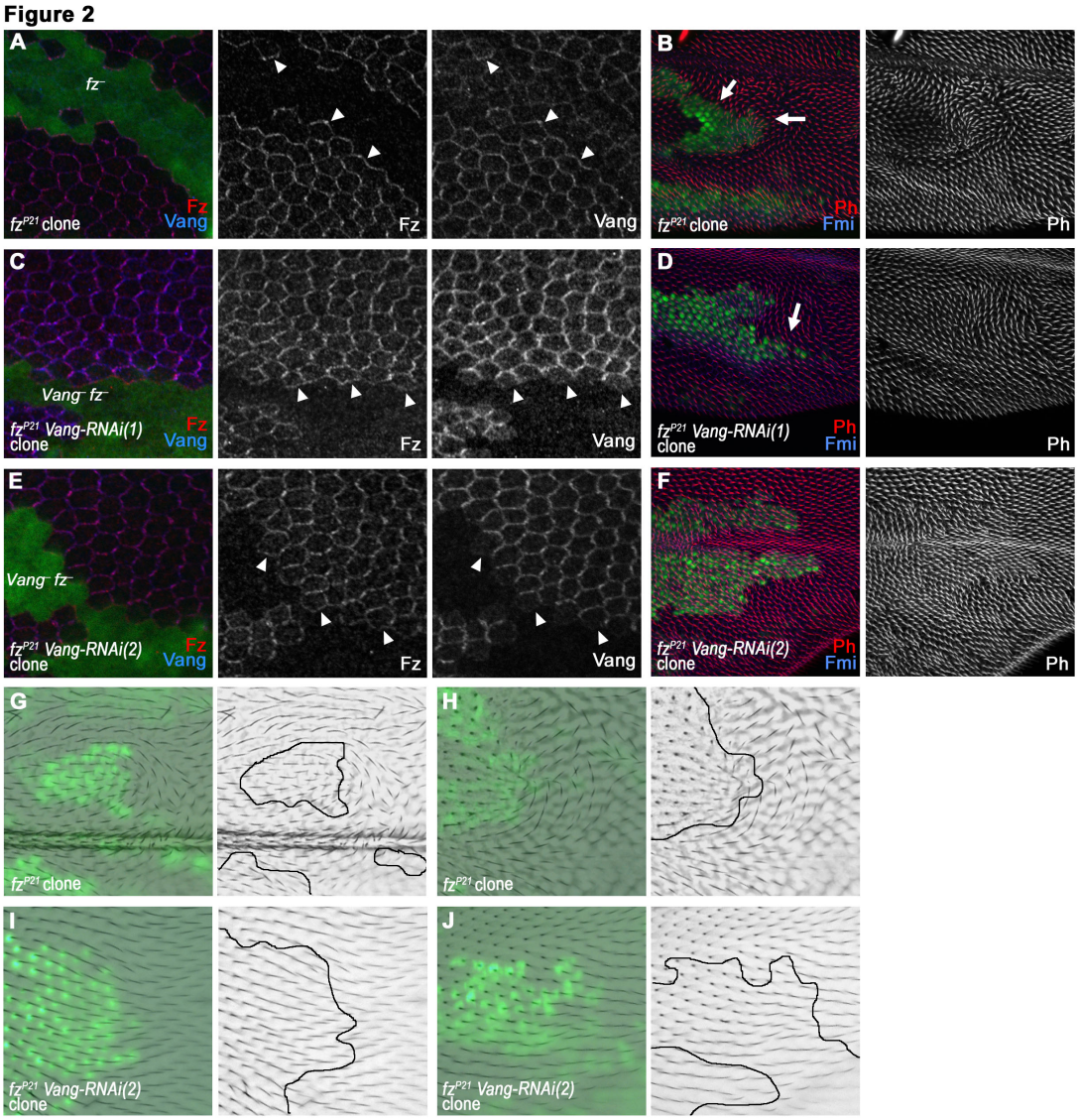

Figure 2. Non-autonomy around *fz*⁻ clones is suppressed by simultaneous RNAi knockdown of *Vang* activity.

(A-F) Pupal wings with loss-of-function clones of fz^{P21} alone (A,B), or fz^{P21} clones also expressing *UAS-Vang-RNAi(1)* (pWIZ line; C,D) or *UAS-Vang-RNAi(2)* (TRiP line; E,F). Wings were immunolabelled for Fz (red) and Vang (blue) at 28 h after pupa formation (APF; A,C,E), or for Phalloidin to mark trichomes (red) and Fmi (blue) at 32.25 h APF (B,D,F). Arrowheads point to clone boundaries where proteins accumulate next to *fz*⁻ clones. Arrows show areas of non-autonomy. GFP (green) positively marks the clones. Representative images from at least 9 clones per genotype are shown.

(G-J) Adult wings with clones of fz^{P21} (G,H) or fz^{P21} *UAS-Vang-RNAi(2)* (TRiP line; I,J). Green nuclei show clone cells and brightfield images show trichomes. Two representative examples from

at least 10 clones are shown for each genotype. All panels are aligned with proximal left and anterior up.

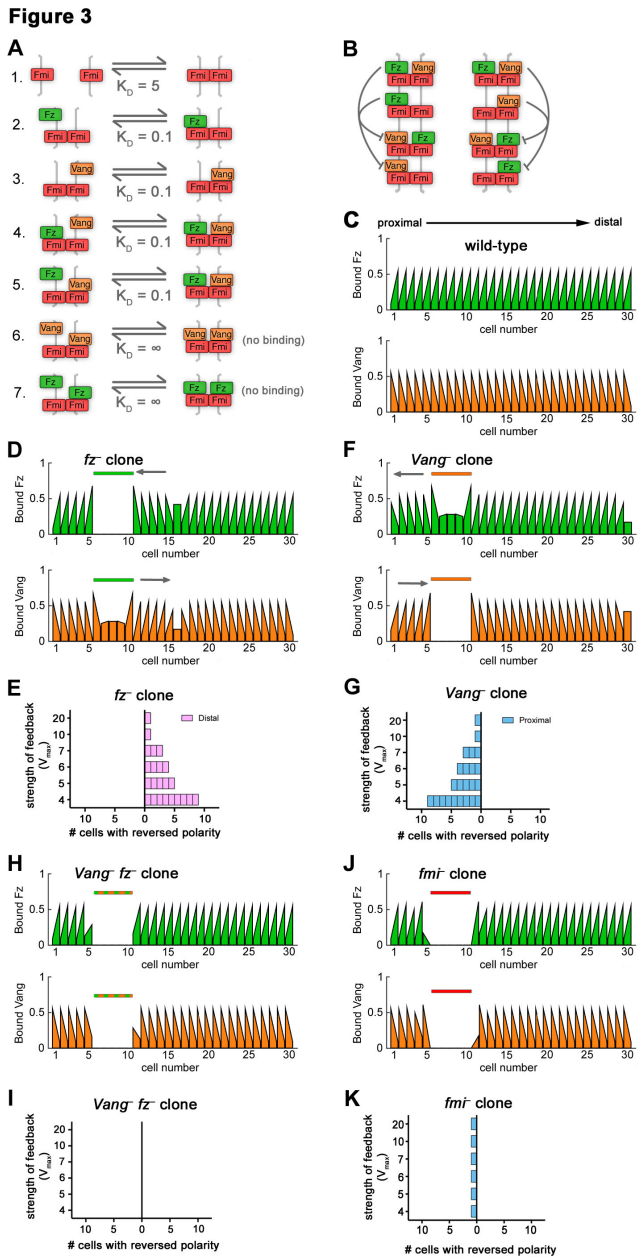

Figure 3. **Simulations of asymmetric complexes with destabilising intracellular feedback interactions show indirect bidirectional signalling.**

(A) Biochemical binding reactions with relative dissociation constants K_D. These K_D values apply to the rest of Fig.3, Fig.S2 and Fig.4. Note that for reactions 6 and 7 no binding occurs due to an on-rate of zero.

(B) Diagram showing bidirectional intracellular destabilising feedbacks between Fz and Vang implemented in this model.

(C,D,F,H,J) Simulation results for one parameter set (Table S1; $V_{max,F} = V_{max,V} = 5$) for wild-type (C) or clones of *fz*⁻ (D), *Vang*⁻ (F), *Vang*⁻ *fz*⁻ (H) or *fmi*⁻ (J). Bound Fz levels (i.e. sum of complexes

that contain Fz within each compartment; upper panels, green graphs) and bound Vang levels (lower panels, orange graphs) are shown for each cell edge. Sloped tops of bars indicate the cell is polarised for that protein. Coloured bars above indicate clone cells (cells 6-10). Grey arrows indicate direction of non-autonomy.

(E,G,I,K) Varying V_{max} parameter (maintaining $V_{max,F} = V_{max,V}$) to alter strength of feedback varies the range of non-autonomous propagation for clones of *fz*$^-$ (E), *Vang*$^-$ (G), but does not alter the number of mispolarised cells around *Vang*$^-$ *fz*$^-$ (I) and *fmi*$^-$ (K) clones. *Vang*$^-$ *fz*$^-$ clones showed no non-autonomy regardless of feedback strength.

Figure 4

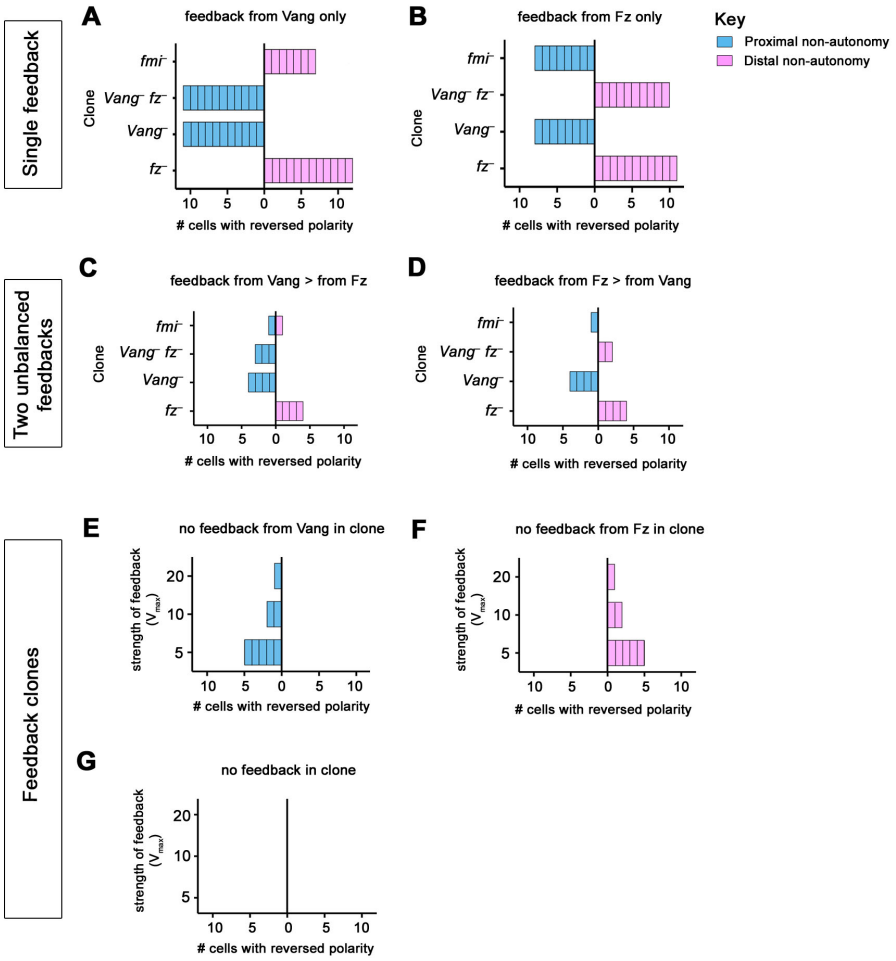

Figure 4. Simulations of asymmetric complexes with single or unbalanced feedbacks show non-autonomy around *Vang*⁻ *fz*⁻ clones.

(A-B) Simulation results for an example parameter set (Table S1) with asymmetric complexes and a single feedback from Vang (A; $V_{max,V}$ = 40, $V_{max,F}$ = 1) or from Fz (B; $V_{max,F}$ = 40, $V_{max,V}$ = 1) operating. The number of cells with reversed polarity around *fz*⁻, *Vang*⁻, *Vang*⁻ *fz*⁻ and *fmi*⁻ clones is quantified.

(C-D) Simulation results with two destabilising feedbacks with different strengths where feedback from Vang is higher (C; $V_{max,V}$ = 8, $V_{max,F}$ = 5) or feedback from Fz is higher (D; $V_{max,F}$ = 8, $V_{max,V}$ = 5). Non-autonomy around *fz*⁻, *Vang*⁻, *Vang*⁻ *fz*⁻ and *fmi*⁻ clones is quantified.

(E-G) Simulation results with feedback interactions altered, but normal protein levels, within clonal cells. Two feedbacks of equal strength (V_{max} = $V_{max,F}$ = $V_{max,V}$) operate in neighbouring wild-type cells, but inside the clone there is only feedback from Vang (E; $V_{max,F}$ = 1, $V_{max,V}$ = V_{max}), only feedback from Fz (F; $V_{max,V}$=1, $V_{max,F}$ = V_{max}) or no feedback (G; $V_{max,F}$ = $V_{max,V}$ = 1). The number of cells with reversed polarity around clones is quantified for each parameter.

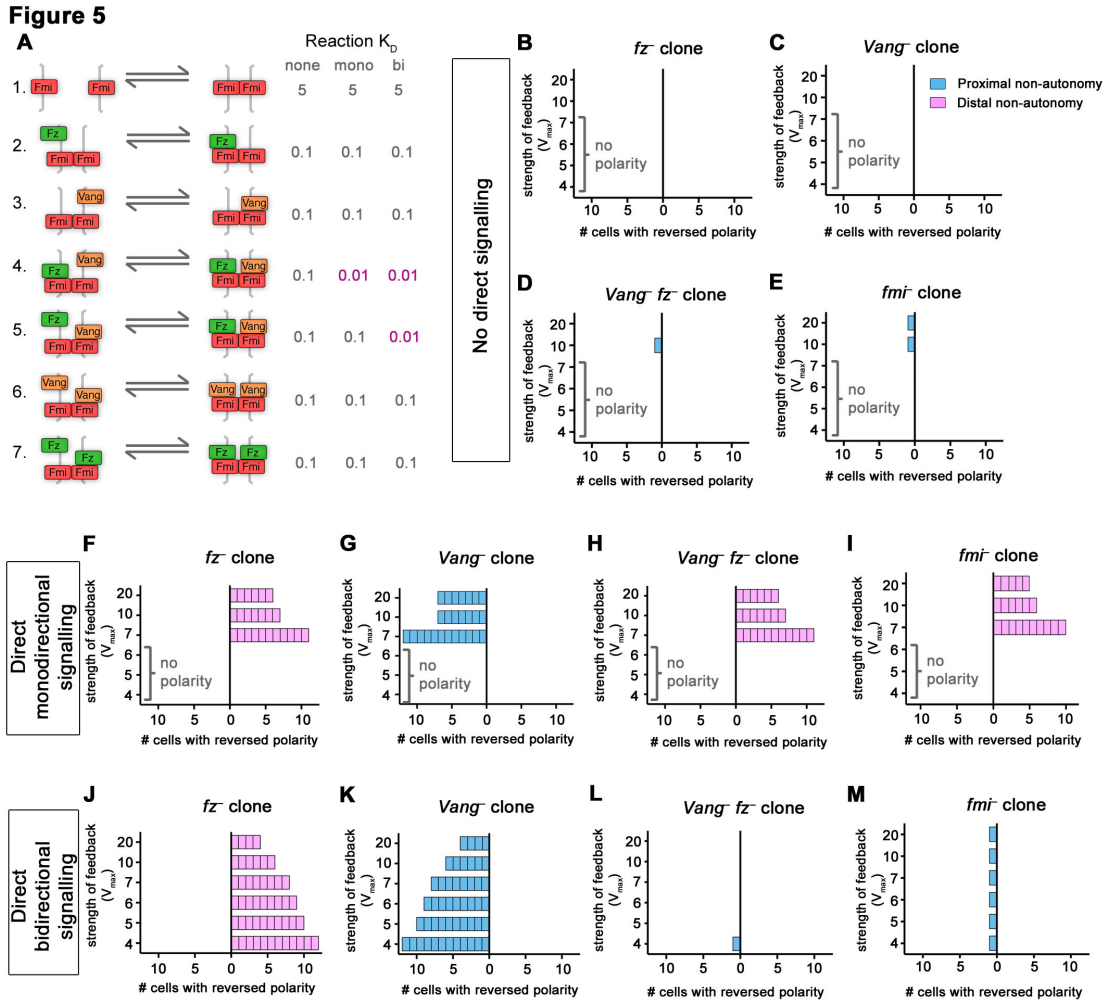

Figure 5. Simulations with symmetric and asymmetric complexes with bidirectional feedback and no direct signalling, direct monodirectional or direct bidirectional signalling

(A) Biochemical binding reactions with relative Dissociation Constants, K_D, for no direct signalling (none; applies to this Figure, panels B-E, and Fig. S5), direct monodirectional (mono; applies to this Figure, panels F-I, and Fig. S6) or direct bidirectional (bi; applies to this Figure, panels J-M, and Fig. S7) signalling.

(B-M) Simulation results varying feedback strength (where $V_{max} = V_{max,F} = V_{max,V}$) for no direct signalling (B-E), direct monodirectional signalling (F-I) or direct bidirectional signalling (J-M). Results shown for *fz*⁻ clones (B,F,J), *Vang*⁻ clones (C,G,K), *Vang*⁻ *fz*⁻ clones (D,H,L) or *fmi*⁻ clones (E,I,M). Parameter conditions where no polarity was observed in the absence of clones are indicated ('no polarity').

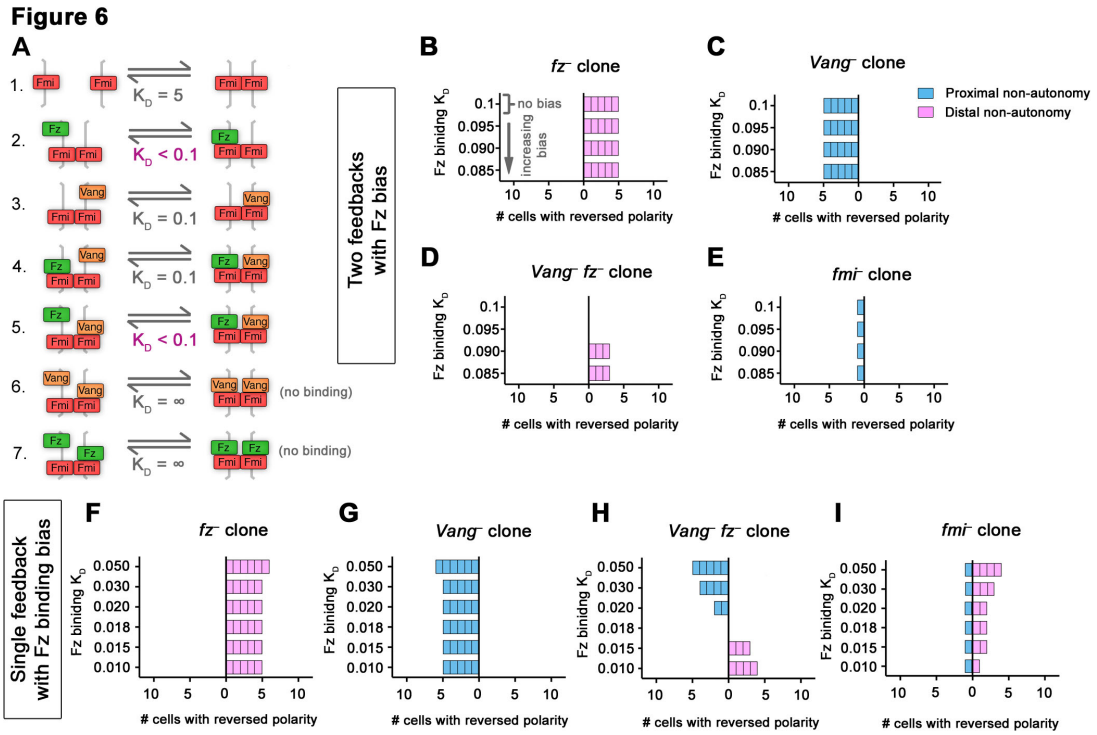

Figure 6. **Biased Fz binding can add directionality to signalling.**

(A) Biochemical reactions with K_D illustrating Fz binding bias, as used for simulations in this Figure and Figure S8. The bias is applied to reactions 2 and 5, which are given a lower K_D than Vang binding reactions. Note that for reactions 6 and 7 no binding occurs due to an on-rate of zero.

(B-E) Simulations with bidirectional feedback interactions ($V_{max,F}$ = $V_{max,V}$ = 5) and varying strengths of a weak Fz binding bias. Numbers are in comparison to the binding rate of Vang, which is 0.1. Number of cells showing non-autonomy around clones of *fz*⁻ (B), *Vang*⁻ (C), *Vang*⁻ *fz*⁻ (D) or *fmi*⁻ (E) is quantified.

(F-I) Simulation results from models with a single feedback from Vang ($V_{max,V}$ = 40, $V_{max,F}$ = 1) and a strong Fz binding bias. Number of cells showing non–autonomy is shown around clones of *fz*⁻ (F), *Vang*⁻ (G), *Vang*⁻ *fz*⁻ (H) or *fmi*⁻ (I).

Table 1

					Clone phenotype			
Complex formation	**Direct signalling (via differential K_D)**	**Model number**	**Feedback interactions**	**Figure**	***fz⁻***	***Vang⁻***	***Vang⁻ fz⁻***	***fmi⁻***
Asymmetric only	none	1	bidirectional (equal strength)	Figure 3; Figure 4E-G	✓	✓	✓	✓
		2	single	Figure 4A,B	✓	✓	×	×
		3	bidirectional (unequal strength)	Figure 4C,D	✓	✓	✓	✓
		-	none	Figure S3	-	-	-	-
	none, but Fmi preferentially binds Fz over Vang (biased binding)	7	bidirectional (equal strength)	Figure 6B-E	✓	✓	✓	✓
		8	single (strong)	Figure 6F-I	✓	✓	✓/×	✓/×
		8	single (weak)	Figure S8D-G	✓	✓	✓/×	✓/×
Asymmetric and symmetric	none	4	bidirectional (equal strength)	Figure 5B-E	×	×	✓	✓
		-	none	Figure S5	-	-	-	-
	monodirectional	5	bidirectional (equal strength)	Figure 5F-I	✓	✓	×	×
		-	none	Figure S6	-	-	-	-
	bidirectional	6	bidirectional (equal strength)	Figure 5J-M	✓	✓	✓	✓
		-	none	Figure S7	-	-	-	-

✓ = model recapitulates non-autonomy direction observed experimentally
× = model does NOT give non-autonomy direction observed experimentally
✓/× = model does not recapitulate all clone conditions for specific parameters

Table 1. Summary of models and results.